Chalcogenide Letters Vol. 18, No. 6, June 2021, p. 311 - 326

Attenuation characteristics of high-energy radiation on As-Se-Sn chalcogenide glassy alloy

Z. M. H. El-Qahtani[a,*], E. R. Shaaban[b], M. M. Soraya[c]
[a]*Physics Department, Faculty of Science, Princess Nourah bint Abdulrahman University, Riyadh, Saudi Arabia.*
[b]*Physics Department, Faculty of Science, Al-Azhar University, Assuit, 71542, Egypt*
[c]*Physics Department, Faculty of Science, Aswan University, Aswan, Egypt*

The present work is mainly interested in the use of chalcogenide glass materials as shielding materials for the highly energetic radiations as X-rays and Gamma rays and particles of high energies as neutrons. The chalcogenide glass system concerned with this study is As_{40}-Se_{60-x}-Sn_x (x = 0, 5, 10, 15, 20 at %). Numerous radiation shielding factors have been deduced by the aid of Phy-X/PSD online software. This software enabled us to achieve the linear and mass attenuation coefficients (LAC, MAC), effective atomic number Z_{eff}, effective electron density, N_{eff}, half-value layer, HVL, tenth value layer TVL, mean free path MEF, energy absorption and exposure buildup factors (EABF, EBF) in photon energy range extended from 0.15 to 15 MeV. The most interesting findings are that the LAC and MAC values are more suitable for shielding purposes than that of some commercial and traditional glasses. Also the results refer to that HVL, TVL, and MFP decrease with the substitution of Selenium by Tin in the tested system, this decreasing is clearer at the medium and high range of photon energies, which indicate to the improvement of shielding features by the adding of Sn to these specimens. Z_{eff} and N_{eff} of these glasses were in the range (33.6- 40.6) and (2.5-2.86 x 10^{23} electrons/g) respectively. The results also point to that EBF and EABF decrease with further raising of Sn-percentage in the investigated chalcogenide system at all the values of MFP at the hole range of the photon energy, that confirm with no doubt that the samples with higher ratios of Tin have better shielding ability than those of lower ratios of Tin in the investigated system. It is also found that FNRCS of the five investigated specimens is in between 0.0886 $Cm^{-1}$and 0.0943 Cm^{-1} that makes them promising protective materials against neutrons, when compared with other commercial and traditional glasses.

(Received April 3, 2021; Accepted June 14, 2021)

Keywords: Chalcogenide glass, As-Se-Sn, Attenuation coefficients, High energetic radiations shielding, Phy-X/PSD software

1. Introduction

For decades, it has become known the existence of high-energy particles and ionizing radiations emitted from radioactive sources. The scientists have made unremitting efforts to study these radiations which resulted in knowing their great importance and promising applications. Scientists have also been able to know the harmful effects of these radiations on the human being and his surrounding environment. To isolate these radiations and protect the human being and surroundings from the harmful effects, many materials have been developed that have good radiation shielding properties. In between these shielding materials were concretes, alloys, rocks and polymers [1-7]. The comparison between the different shielding materials is based on many factors, including high efficiency, low cost, high flexibility in manufacturing them to take different forms, transparency, and the toxicity effects that make them harmful in themselves. Recently a lot of researches have been done to develop different materials for best radiations shielding [8-16], the majority of these researches are directed to the oxide glasses due to the high efficiency for shielding and their optical transparency, in addition to low cost for manufacturing. In the recent

* Corresponding author: somahmoud_81@yahoo.com
https://doi.org/10.15251/CL.2021.186.311

two years, a new motivation of studying chalcogenide glasses as shielding due to their attractive physical properties as their high transparency, high density, high atomic number, flexibility, high resistance against corrosion, good thermal stability and easy to use and prepare with various techniques. The shielding parameters of both chalcogenide-ceramic [17], chalcogenide glass heavy metal halide [18] have been estimated and the most recent work until now according to searching on science direct website have been presented by Imen Kebaili et al on the protection features of Se-Ge-Sb-Ag chalcogenides [19]. From these studies of radiation shielding on chalcogenides, it was found that these materials are better than many of ordinary and commercial glasses and also better than many of the recently developed oxide glasses [17-19]. An experimental valuable study were developed by Ankita Srivastava et al about the radiation-induced effects of Gamma rays on Se78Te20Sn2 [20], thermal analysis has confirmed the stability of these materials against recrystallization when exposed to gamma rays and stability against aging effects induced by gamma rays, a slight increase of modulus of elasticity and the microhardness were observed. Also the dielectric features were found to be stable against gamma radiation at high energies except an abnormal increase in dielectric loss at low energies side [20]. For all of these positive features, Ankita Srivastava et al have considered these materials as promising candidate for radiation shielding materials for preventing workers from the harmful effects of nuclear wastes [20]. Theoretically various calculations programs have been developed to deduce the shielding factors and hence describe how much the material is suitable to prevent from harmful radiations. Among these programs, Monte Carlo and XCOM simulation codes such as FLUKA and x Geant4 [21–27]. Recently the researchers have developed Phy-X/PSD free online program that can determine the different shielding parameters in different ranges of the photon energy [28]. Many authors have studied the shielding features of different materials upon the use of this program [18, 29, 30]. In current work, we have deduced the shielding factors of varies compositions of As_{40}-Se_{60-x}-Sn_x (x = 0, 5, 10, 15, 20 at %) chalcogenides by the aid of Phy-X/PSD online software [28] since LAC, MAC, Z_{eff}, N_{eff}, HVL, TVL, MFP, EABF and EBF buildup factors, fast neutron cross section FNRCS and other shielding parameters have been estimated in the range of photon energy between 0.15 MeV to 15 MeV.

2. Materials and methods

We have studied before in a previous work the induced structural and optical effects of substitution of Selenium by Tin in the As_{40}-Se_{60-x}-Sn_x (x = 0, 5, 10, 15, 20 at %) chalcogenid alloys system [31]. The results of this research paper have referred to the increasing of refractive index and dielectric constants while the decreasing of the energy gap with the addition of Sn to As-Se-Sn chalcogenide glass system. Also the theoretically physical parameters like average heat of atomization, average coordination number, lone pairs electrons numbers, and cohesive energy have been calculated; these parameters were increased with increasing the Sn ratio in the investigated system, which may attributed to increasing the glass stability of these composition [31]. The densities (in gm/cm^3) of the various compositions of As_{40}-Se_{60-x}-Sn_x (x = 0- 20 at %) alloys were estimated. The Phy-X/PSD online program was used to extract the radiation shielding parameters in the photon energy between 0.015 and 15 MeV. Table 1 lists the tested compositions, their abbreviated names, and their densities. The estimated densities (gm/cm^3) were inputted into the program and the corresponding chemical formula of each sample.

Table 1. The tested compositions As_{40}-Se_{60-x}-Sn_x (x = 0, 5, 10, 15, 20 at %), their abbreviated names, and their densities.

Sample no.	Name	code	density
1	$As_{40}Se_{60}$	ASS1	5.174
2	$As_{40}Se_{55}Sn_5$	ASS2	5.349
3	$As_{40}Se_{50}Sn_{10}$	ASS3	5.515
4	$As_{40}Se_{45}Sn_{15}$	ASS4	5.673
5	$As_{40}Se_{40}Sn_{20}$	ASS5	5.824

3. Theoretical relations

The Beer-Lambert relationship, which defines the relationship between the transmitted radiation intensity, I and the incident radiation intensity, I_o as a photon of a single energy travelling across the material is written as [32]:

$$I = I_0 e^{-\mu d}\ , \tag{1}$$

Since μ (cm^{-1}) is the LAC and d (in cm) is the tested sample thickness. The MAC (μ_m, in cm^2/g) describes the interactions possibility, between the incident high energetic photons of Gamma or X- Rays and mass of the unit area for a given material [32]:

$$\mu_m = \left(\frac{\mu}{\rho}\right) = - \frac{\ln(I/I_0)}{\rho d} = - \frac{\ln(I/I_0)}{d_m}\ , \tag{2}$$

d_m (in g/cm^2) here is the mass thickness of the specimen, and ρ (g/cm^3) gives the material density. The next relationship gives the μ_m for a specimen [32]

$$\mu_m = \left(\frac{\mu}{\rho}\right) = \sum_j w_j \left(\frac{\mu}{\rho}\right)_j\ , \tag{3}$$

w_j is the fraction of the weight of the j^{th} included element. *HVL*, and *TVL* the tenth value layer define the necessary thickness to attenuate the incident photons intensity to its half and tenth values, they are written as [28].

$$HVL = \frac{\ln(2)}{\mu}\ ,\ TVL = \frac{\ln(10)}{\mu}\ , \tag{4}$$

The *MFP*, describe the average travelled distance doing by a photon between two successive collisions with the electrons or nucleus of the material and it is defined as following [28]:

$$MFP = \frac{1}{\mu}\ , \tag{5}$$

The Z_{eff} of the matter characterized by the next formula [28]:

$$Z_{eff} = \frac{\sigma_a}{\sigma_e}, \tag{6}$$

σ_a *(in* cm^2/gm) here is the total atomic cross-sections, and it is related to the mass attenuation coefficients μ_m in term of the next relationship [28]:

$$\sigma_a = \frac{N\mu_m}{N_A}, \tag{7}$$

since N_A is the Avogadro number, and σ_e*(in* cm^2/gm*) is* the total electronic cross-sections, and it is described by the relation [33]:

$$\sigma_e = \frac{1}{N_A}\left(\sum_j \frac{f_j A_j}{Z_j}(\mu_m)_j\right), \tag{8}$$

Aj, f_j and Z_j are the atomic weight, mole fraction and atomic number, of the j^{th} involved element. The effective number of electrons N_{eff} (in electrons/kg) is written as [34]:

$$N_{eff} = \frac{N_A}{N} Z_{eff} \sum_j n_j = \frac{\mu_m}{\sigma_e}, \tag{9}$$

where $\sum n_j$ represent the totally numbers of involved elements in the tested sample. Effective conductivity (C_{eff} ; in S/m) characterized by the next formula [35]

$$C_{eff} = \left(\frac{N_{eff}\rho e^2 \tau}{m_e}\right)10^3, \tag{10}$$

since e and m_e are the electronic charge and mass, τ is the electron average lifetime at the Fermi Surface.

According to Sakar and coworkers [28] The equivalent atomic number Z_{eq} can be achieved from R, the ratio of Compton partial mass attenuation coefficient to the total mass attenuation coefficient at a certain photon energy, from the relationship:

$$Z_{eq} = \frac{Z_1(\log R_2 - \log R) + Z_2(\log R - \log R_1)}{\log R_2 - \log R_1}, \tag{11}$$

Z_1 and Z_2 are the elements atomic numbers in correspondence with the ratios R_1 and R_2, Z_{eq} values of the material is used in the interpolatationof G-P fitting parameters in the photon energy between 0.015 MeV and 15 MeV. The G-P fitting parameters can be estimated according to interpolation next formula [36, 37].

$$P = \left[P_1(\log Z_2 - \log Z_{eq}) + P_2(\log Z_{eq} - \log Z_1)\right]\left(\log \frac{Z_1}{Z_2}\right), \tag{12}$$

The build-up factors (*EBF* and *EABF*) can be achieved using the G-P fitting parameters according to the equations:

$$B(E,X)=\begin{Bmatrix}1+\dfrac{(b-1)(K^{X}-1)}{(K-1)} & \text{for K}\neq 1\\ 1+(\text{b-1})\text{X} & \text{for K=1}\end{Bmatrix}, \tag{13}$$

E and *X* represent primary photon energy and penetration depth. The function *K* (*E, X*) can be estimated according to the equation:

$$K(E,X)=cX^{a}+d\left[\left(X/X_{K}\right)-2-\tanh(-2)\right]\left(1-\tanh(-2)\right)^{-1}, \tag{14}$$

The neutrons which are defined as subatomic particles with a neutral charge, neutrons may interact with a medium through neutron capture, nuclear fission, elastic and inelastic scattering and nuclear spallation processes. The fast neutron removal cross section (FNRCS) (ΣR) is a factor used to characterize how far the material is capable to attenuate neutrons. FNRCS is defined as:-

$$\sum R=\sum_{i}\rho_{i}\left(\sum R/\rho\right)_{i} \tag{15}$$

Here, ρ_i *is* the partial density and $(\Sigma R/\rho)_i$ is the mass removal cross section (MRCS) of the ith involved element, respectively [38]. MRCS of the constituent elements were gotten by the aid of the literature [39, 40].

4. Results and discussions

The radiation shielding properties represented by specified parameters have been estimated in the region of photon energy possess between 0.15 MeV and 15 MeV in accordance with Phy-X/PSD Program.

3.1. MAC and LAC of As_{40}-Se_{60-x}-Sn_x chalcogenide glass

The photon attenuation factors provide important knowledge for understanding the shielding characteristics of highly energetic radiations as gamma rays and X-rays. Fig. 1 shows the *MAC* variation versus photon energy (0.15 - 15 MeV) for the tested chalcogenide glasses. This graph shows that the largest values of MAC lies at the low photon energies (*E* = 0.015 and 0.02 MeV), thus MAC values varies between 101.4 and 85.8 Cm^2/gm at 0.015 MeV and between 47.2 and 39.9 Cm^2/gm at 0.02 MeV as the doping of Tin increases from 0 to 20 % that may be discussed in terms of photoelectric effect K-absorption edge of the constituent elements (see Table 2 [41]). After that, MAC decreases sharply (between 22.7-0.22 Cm^2/gm in the ASS5 and between 15.6 – 0.17 Cm^2/gm in ASS1) as the photon energy changes from 0.03 – 0.2 MeV, in this region the specimens with higher ratio of Tin have highest values of MAC. In the medium photon energy region 0.3 – 2 MeV, an exponential behavior of these plots were detected, thus the MAC decreases from 0.128 - 0.041cm^2/gm approximately and the doping effect is unnoticeable in this region. Besides, at higher range of photon energies (3-15 MeV), MAC values show a plateau behavior (0.036 - 0.037 cm^2/gm approximately for all the specimens under investigation, ASS1-ASS5).

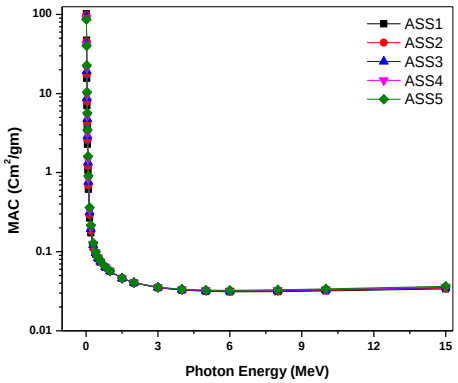

Fig. 1. The mass attenuation coefficients (MAC) values of the studied chalcogenide glasses (ASS1-ASS5) as a function of photon energies range (0.15 - 15 MeV).

Table 2. The atomic number Z and photon energies (MeV) of the absorption edges of the involved elements under study [41].

Element	Z	L3	L2	L1	K
Se	34	1.43580E-03	1.47620E-03	1.65390E-03	1.26578E-02
As	33	1.32310E-03	1.35860E-03	1.52650E-03	1. 18667E-02
Sn	50	3.92880E-03	4.15610E- 03	4.46470E-03	2.92001E-02

The interaction of highly energetic photons with the matter is mainly depending on both the atomic number (Z) of the target material and the incident photons energies in distinct dominant interaction processes at various energies of the photon. At low energies, photoelectric absorption (PE) is the dominant process, in the intermediate energies, the most favorable is Compton scattering (CS), and at high energies, the pair production (PP) process has the highest probability to occur. Since, the *MAC* plots of the tested chalcogenide glass have its highest values in photoelectric effect energy region.

Fig. 2 illustrates the *LAC* variation of the studied samples (ASS1-ASS5) versus the photon energies. *LAC* varies between (524.8-0.18 Cm^{-1} approximately) across the variation of photon energy range (0.15-15 MeV). *LAC* variation has the same trend as MAC, hence they are dependent on each other. *LAC* graphs can be interpreted in the same way as MAC.

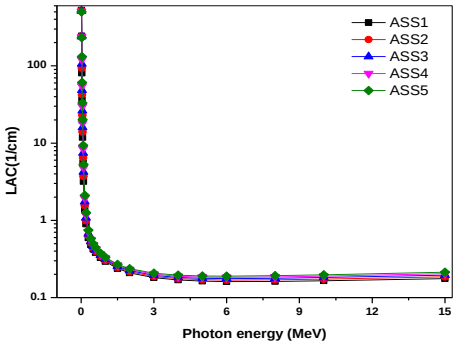

Fig. 2. The linear attenuation coefficients (LAC) values of the investigated chalcogenide glasses (ASS1-ASS5) against photon energies range (0.15 - 15 MeV).

Table 3 shows results of *LAC* values of the tested compositions (ASS1-ASS5) that have good shielding competence against that of some commercial glasses [42]. Also, the values of *LAC* and *MAC* are larger and thereafter much better for shielding than that of some traditional glasses as

basalt- magnetite, steel-scrap, ilmanite-limonite, hematite-serpentine, ilmanite, steel-magnetite, and concretes [43].

Table 3. The linear attenuation coefficient (in Cm^{-1}) of the tested compositions (ASS1-ASS5) against some commercial glasses at different photon energies (in MeV) [42].

Energy in MeV	LAC (Cm^{-1})	RS-253	RS 253-G18	RS 323-G19	RS-360	RS-520	ASS1	ASS2	ASS3	ASS4	ASS5
0.2		0.32	0.33	1.25	1.72	3.54	0.897	0.988	1.078	1.167	1.256
0.662		0.19	0.19	0.28	0.32	0.5	0.383	0.399	0.414	0.429	0.443
1.25		0.14	0.14	0.18	0.21	0.3	0.258	0.267	0.275	0.284	0.294

3.2. HVL, TVL, MFP of As-Se-Sn chalcogenide glass

As mentioned before, *HVL, TVL, and MFP* are inversely related on *LAC* values. Figs. 3, 4 illustrate *HVL* and *TVL* variations against photon energy in the range between 0.015 and 15 MeV. These plots show that the lowest values of *HVL* and *TVL* lie at the lowest photon energy, then they sharply increase until reaching to 1.5 MeV, followed by a slower rate of increasing up to 3 MeV. After that, *HVL* and *TVL* behavior begin to have nearly stationary plot in the higher energies up to 15 MeV. These findings should be interpreted in terms of the main processes of photon interactions with matter; PE, CE, and PP as discussed before.

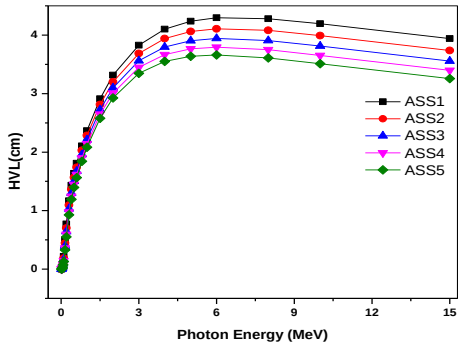

Fig. 3. Half value layer (HVL) of the selected chalcogenide glasses (ASS1-ASS5) versus photon energies range (0.15 - 15 MeV).

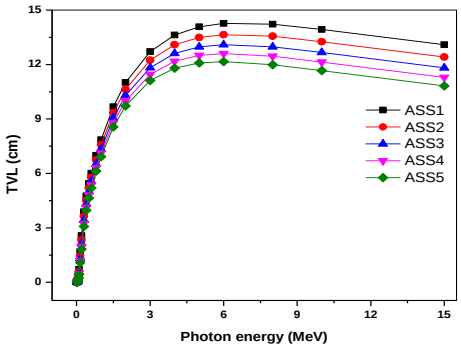

Fig. 4. Tenth value layer (TVL) of the chalcogenide glasses (ASS1-ASS5) against photon energies range (0.15 - 15 MeV).

It is worth clarifying now that the specimens of higher ratios of Tin have the lowest values of *HVL* and *TVL*, this behavior appears more evident in the nearly intermediate and high energies of the photon (1- 15 MeV). Thus the lowest values of *HVL* and *TVL* were declared to ASS5, i.e, the sample of higher ratios of Tin. These results, confirm that the increasing of Tin in the (ASS1-ASS5) chalcogenide glass improves the shielding factors, especially at intermediate and higher energies of the photon.

Fig. 5 represents the MFP graph versus photon energy (0.015-15 MeV). This figure illustrates the same trend as TVL and HVL. Since *MFP*, *HVL*, *TVL* are inversely depending on *LAC*, then MFP behavior become more obvious according to the previous interpretation. Increasing Tin ratios in the As-Se-Sn chalcogenide glass system decrease the MFP values especially at intermediate and higher photon energies.

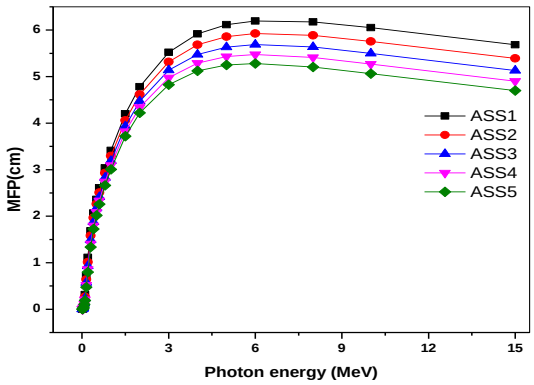

Fig. 5. The mean free path (MFP) variations of the chalcogenide glasses (ASS1-ASS5) under study with photon energies range (0.15 - 15 MeV).

Figs. 6 and 7 represent useful comparisons of HVL and MFP of As-Se-Sn glasses (ASS1-ASS5) with other commercial and traditional glasses [28]. Figs. 6 and 7 illustrate that HVL and MFP of the investigated chalcogenide glasses have lower values than the traditional glasses (Chromite, Ferrite, Magnetite and Barite) and some commercial glasses (RS-360 and RS-253-G18) especially at the intermediate and higher energies of the photon. These findings emphasize the better shielding characteristic of our chalcogenide glasses (ASS1-ASS5) than the previously mentioned traditional and commercial glasses.

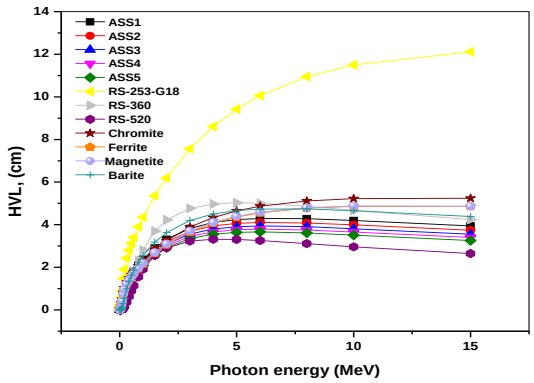

Fig. 6. Half value layer (HVL) of the selected chalcogenide glasses (ASS1-ASS5) and other traditional and commercial glasses versus photon energies range (0.15 - 15 MeV).

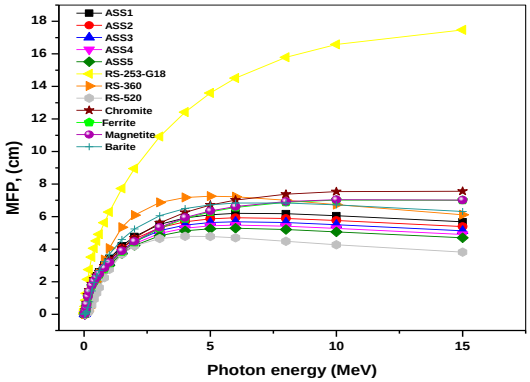

Fig. 7. The mean free path (MFP) variations of the chalcogenide glasses (ASS1-ASS5) under study and other ordinary and commercial glasses against photon energies range (0.15 - 15 MeV).

3.3. ACS and ECS of As-Se-Sn chalcogenide glass

The ACS and ECS define the material unit volume interaction probability per atom and per electron, respectively. High values of ACS and ECS refer to good radiation shielding parameters. Figs. (8, 9) display respectively, ACS and ECS measurements of As-Se-Sn chalcogenide glass as a function of photon energy (0.015-15 MeV). ECS and ACS have higher values at the lower photon energies. ACS varies in the range (1.3E-20 - 5.18 E-24) and ECS changes between (3.88E-22 - 1.38E-25 cm^2/gm) in the As-Se-Sn system under investigation. ECS and ACS plots show a sharp decrease until reaching to 0.2 MeV of the photon energy. The plots then show a slower rate of decreasing at the intermediate region of photon energy (0.3-2 MeV). At higher energies (3- 15 Mev) these plots show nearly stationary behavior. These results can be discussed also in terms of the occurrence probability of the main interaction processes PE, CE and PP.

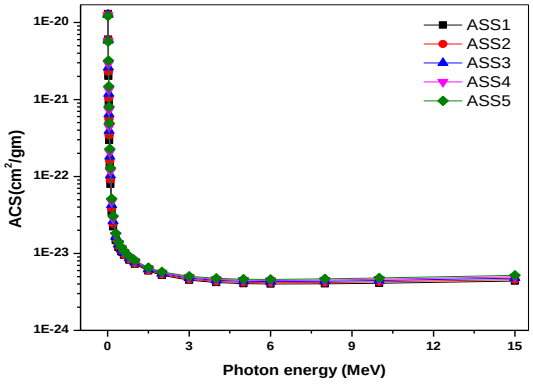

Fig. 8. The total atomic cross section (ACS) of (ASS1-ASS5) chalcogenide glasses versus photon energies range (0.15 - 15 MeV).

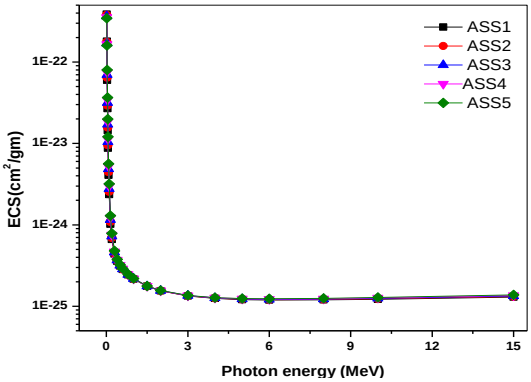

Fig. 9. The total electronic cross section ECS of the chalcogenide glasses (ASS1-ASS5) under investigation as a function of photon energies range (0.15 - 15 MeV).

3.4. N_{eff}, Z_{eff} and C_{eff} of As-Se-Sn chalcogenide glass

Fig. 10 displays Z_{eff} of the tested specimen as a function of photon energy. Z_{eff} for all the investigated samples (ASS1-ASS5) have its lowest values at 0.02 MeV. After that Z_{eff} increases suddenly until reaching to their highest values (40.56 -33.62) at 0.06 MeV for (ASS1-ASS5) glasses; then, they sharply decrease with rising the energies up to 0.4 MeV. In the photon energy between 0.5 and 1 MeV, an exponential decrease is shown. Z_{eff} begin to show approximately constant behavior in the photon energy range (1.5-15 MeV). This described trend of Z_{eff} is in accordance with all the investigated glasses except ASS1 which show almost stationary behavior at all regions of photon energies (Z_{eff} of ASS1 is 33.62-33.6 in the photon energy range 0.15-15 MeV). It is obviously shown that the samples with the largest doping of Tin have the highest values of Z_{eff} at the whole energy ranges. Z_{eff} give a measure of how much the photons interact with a particular material, i.e., reducing the energies of the photon. Thus one can say that the material of highest values of Z_{eff} has the highest efficiency for radiation shielding.

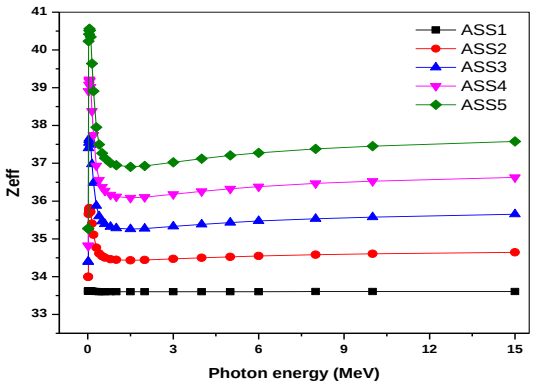

Fig. 10. Effective atomic number (Z_{eff}) of the chalcogenide glasses (ASS1-ASS5) under study against photon energies range (0.15 - 15 MeV).

Moreover, N_{eff} which is directly dependent on Z_{eff} is represented versus photon energies, in Fig. 11. It is clear in this figure that N_{eff} has a similar behavior of Z_{eff}. However, at low energies 0.015 and 0.02 MeV, the lowest doped specimens with Tin has the highest values of N_{eff} (these values of photon energies (0.015 and 0.02 eV) are approximately corresponding to *K*-absorption edges of Selenium and Arsenic, i.e the more concentrated elements in the tested compositions).

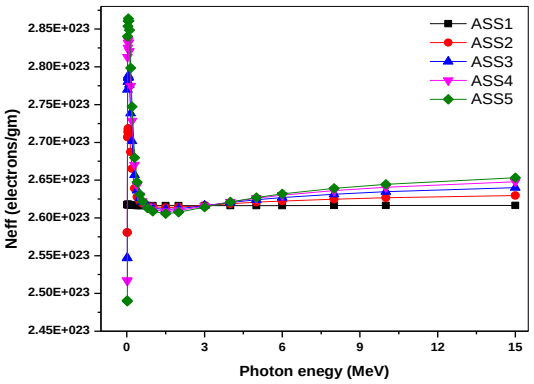

Fig. 11. Effective electron density (N_{eff}) of the studied chalcogenide glasses (ASS1-ASS5) versus photon energies range (0.15 - 15 MeV).

Effective conductivity (C_{eff}) is displayed in Fig. 12, it have similar trend of Z_{eff}, hence it is directly dependent on N_{eff} , and subsequently dependent on Z_{eff} . It is obviously shown that C_{eff} increases with increasing Tin ratio within the investigated specimens. In a previous work we have deduced in As-Se-Sn that increasing Sn content within the samples increase numbers of free electrons [31].

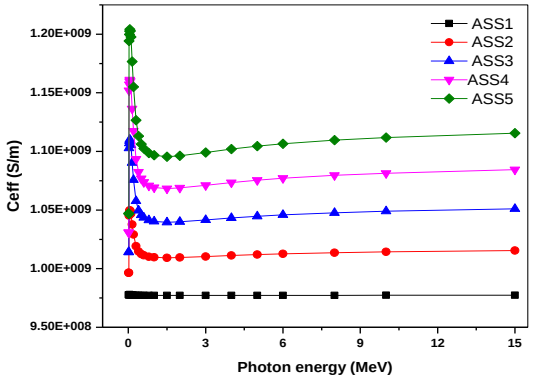

Fig. 12. Effective conductivity (C_{eff} ; S/m) of (ASS1-ASS5) with photon energies range (0.15 - 15 MeV).

3.5. R (the ratio (μ/ρ) Compton/(μ/ρ) total), Z_{eq} (equivalent atomic number) of As-Se-Sn chalcogenide glass

The *R* which is defined as the ratio $(\mu/\rho)_{Compton}/(\mu/\rho)_{total}$, is displayed in Fig. 13 versus photon energy (0.015-15 MeV). It is obviously shown that the highest value of *R* for the tested compositions lie in the intermediate energy region at 1 MeV. In this range of energy, Compton Effect process is the more expected process to occur. As mentioned before Z_{eq}, depends on *R* and it is represented in Fig. 14 against the studied range of photon energies. The figure shows that Z_{eq} has its lowest values at 0.015 MeV. Then these plots increase suddenly until reaching to their highest values at 1 MeV. After that, the curves decrease slowly until reaching to a plateau at the high energy region. It is clear that the compositions with higher Tin doping have higher values of Z_{eq} at the intermediate and high energies of the photon, where the CE and PP processes are the dominances. However, at 0.015 MeV, ASS1 has the highest value of Z_{eq} and ASS5 has the lowest (at 0.015 MeV, which is nearly around the PE *K*-absorption edges of the more contributed elements Se- and As).

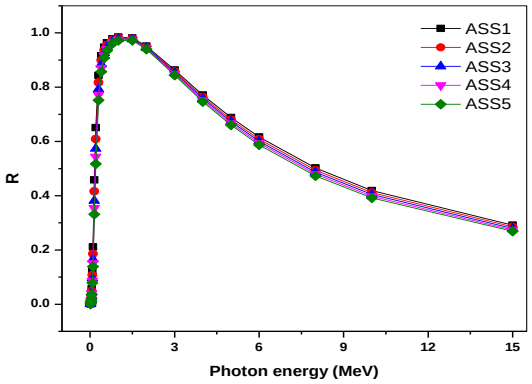

Fig. 13. The ratio (μ/ρ) Compton/(μ/ρ)Total (R) of the investigated chalcogenide glasses (ASS1-ASS5) as a function of photon energies range (0.15 - 15 MeV).

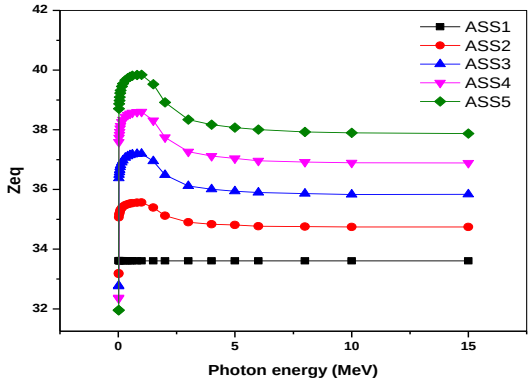

Fig. 14. The equivalent atomic number (Z_{eq}) of the studied chalcogenide glasses (ASS1-ASS5) versus photon energies range (0.15 - 15 MeV).

3.6. Energy exposure buildup factor (EBF) and Energy absorption buildup factor (EABF) of As-Se- Sn chalcogenide glass.

EBF and EABF are displayed against photon energy at various values of MFP (0.5 - 40). Figs. 15 (a-c) and Figs. 16 (a-c) represent the EBF and EABF for (ASS1, ASS3, ASS5), respectively. All these plots show that the higher values of EBF and EABF are corresponding to the higher values of MFP. At 0.02 and 0.06 MeV, *EFB* and EABF take their highest values for all values of MFP. It is shown that the lowest values of EBF and EABF lie at 0.015, 0.05 and 0.1 MeV (around *K*-absorption edges of the involved elements and before the reaching to the effective region of CE process). This trend can be described in terms of the probability of occurrence for the various photon interaction processes so that the larger number of photons will be absorbed. Therefore, EABF and EBF were reduced. But at the medium energy region, (where, the CE is the dominance process), EBF and EABF start to increase because of the enhancing of the photon scattering process due to CE which couldn't completely take off the photon. Thereafter, the lifetime of the photon becomes longer, which increase its probability to migrate from the material. Also, EBF and EABF start to show another increasing in the high energy region (4 - 15 MeV) which attributed to the multiple scattering processes which enhance the buildup of secondary gamma photons due to electron-positron destruction.

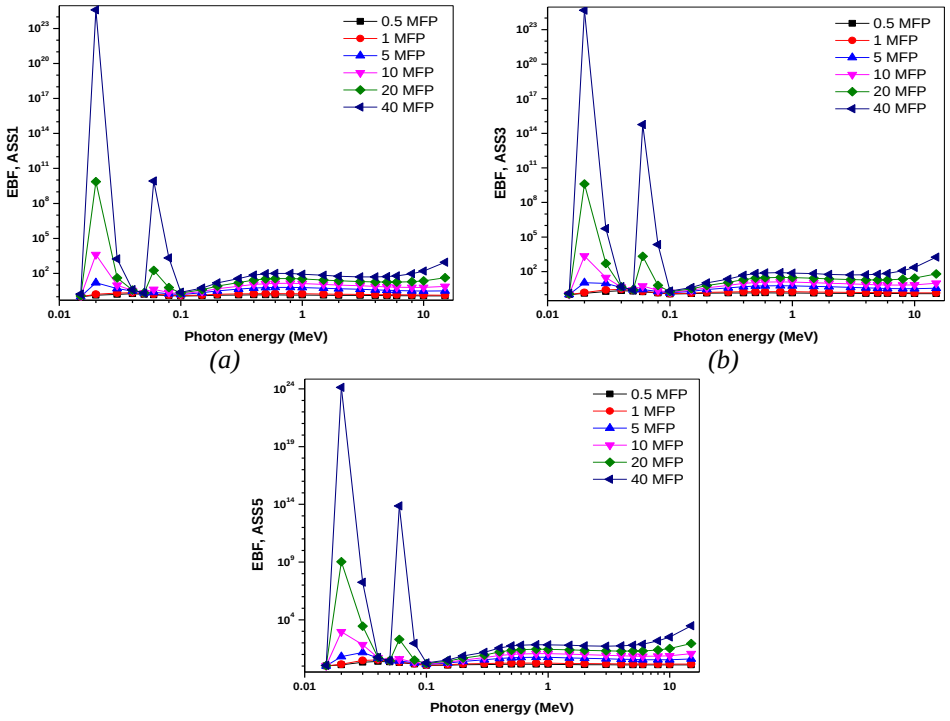

Fig. 15. (a-c) Energy exposure build up factor (EBF) of the selected chalcogenide glasses (ASS1-ASS5) as a function of photon energies range (0.15 - 15 MeV).

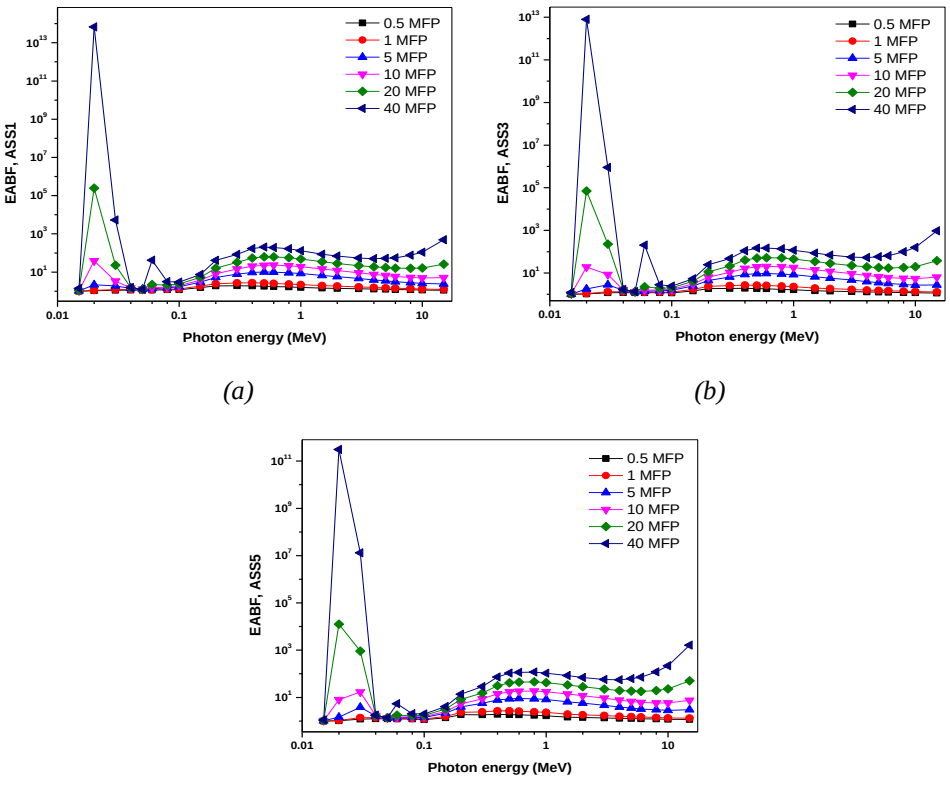

Fig. 16. (a-c) Energy absorption build up factor EABF of the studied chalcogenide glasses (ASS1-ASS5) as a function of photon energies range (0.15 - 15 MeV).

It is worth noting that EBF and EABF decrease with increasing Sn doping level within the tested compositions at all the photon energies at all the MFP values, which give strong evidence about improvement of shielding characteristics with inserting Tin at the expense of Selenium in these investigated compositions.

3.7. FNRCS of As-Se-Sn glasses

Fig. 17 shows the FNRCS of the tested glasses in comparison with other commercial and traditional glasses. FNRCS of the investigated samples (ASS1, ASS2, ASS3, ASS4, ASS5) were (0.089, 0.09, 0.092, 0.093, 0.094 Cm^{-1}) respectively. It is clearly within the graph that FNRCS of ASS1-ASS5 glasses are higher and therefore better than RS-360, RS-253-G18 and RS-520, however they are lower than Chromite, Ferrite, Magnetite and Barite. It is also noticed that the increment of Sn enhance the shielding properties of these glasses throughout increasing FNRCS, which attributed to the larger atomic number and density of Sn in comparison with that of Se (see Table 1).

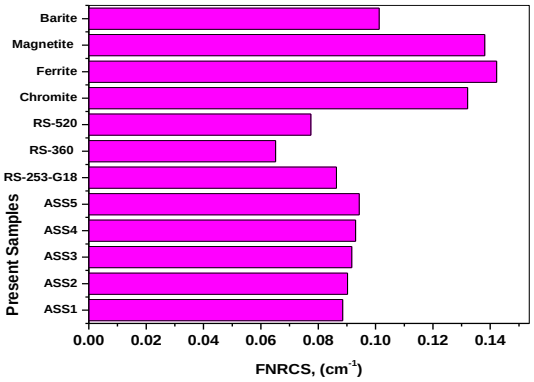

Fig. 17. The fast neutron removal cross section, FNRCS of the studied chalcogenide glasses (ASS1-ASS5) in comparison with FNRCS of other traditional and commercial glasses.

4. Conclusions

The radiation shielding factors for various compositions of As_{40}-Se_{60-x}-Sn_x (x = 0, 5, 10, 15, 20 at %) have been deduced using in the photon energy range (0.15 - 15 MeV). The findings refer to that the LAC and MAC values are larger and then better than some traditional and commercial glasses. HVL, TVL, and MFP decrease with increasing Sn in the investigated samples at the intermediate and high energies of the photon. Z_{eff} was found to increase with increasing Sn within the studied samples which was attributed to the atomic numbers and atomic weights of the constituting elements.

EBF and EABF values were increased with increasing MFP at all the photon energy region, while they were decreased with increasing tin concentration within the tested glasses at all the photon energy range. The estimated values of FNRCS are varied from 0.089 to 0.094 Cm^{-1}. All of these results make the investigated system better neutrons and Gamma rays protection than some ordinary and commercial glasses.

Acknowledgments

This research was funded by the Deanship of Scientific Research at Princess Nourah bint Abdulrahman University through the Fast-track Research Funding Program.

References

[1] V. Singh, S. Shirmardi, M. Medhat, N. Badiger, Vacuum **119**, 284 (2015).
[2] J. Singh, H. Singh, J. Sharma, T. Singh, P. S. Singh, Progress in Nuclear Energy **106**, 387 (2018).
[3] M. Sayyed, G. Lakshminarayana, I. Kityk, M. Mahdi, Radiation Physics and Chemistry **139**, 33 (2017).
[4] K. Mahmoud, M. Sayyed, O. Tashlykov, Nuclear Engineering and Technology **51**, 1835 (2019).
[5] Asmaa Mansour, M. I. Sayyed, K. A. Mahmoud, Erdem Şakar, E. G. Kovaleva, Journal of Radiation Research and Applied Sciences **13**(1), 94 (2020).
[6] Y. Rammah, K. Mahmoud, M. Sayyed, F. El-Agawany, R. El-Mallawany, Journal of Non-Crystalline Solids **534**, 119944 (2020).
[7] K. A. Mahmoud, O. L. Tashlykov, A. F. E. Wakil, H. M. H. Zakaly, I. E. E. Aassy, AIP Conference Proceedings **2174**, 020036 (2019).
[8] A. Goel, E. R. Shaaban, D. U. Tulyaganov, J. M. F. Ferreira, Journal of the American Ceramic Society 91 (8), 2690 (2008).
[9] K. Mahmoud, E. Lacomme, M. Sayyed, Ö. Özpolat, O. Tashlykov, Heliyon **6**, e03560 (2020).
[10] A. Kumar, D. Gaikwad, S. S. Obaid, H. Tekin, O. Agar, M. Sayyed, Progress in Nuclear Energy **119**, 103047 (2020).
[11] H. Tekin, L. Kassab, S. A. Issa, M. Martins, L. Bontempo, G. R. da Silva Mattos, Ceramics International, 2020.
[12] B. Alım, Applied Physics A **126**, 1 (2020).
[13] E. Şakar, Ö. F. Özpolat, B. Alım, M. Sayyed, M. Kurudirek, Radiation Physics and Chemistry **166**, 108496 (2020).
[14] A. Abouhaswa, M. Al-Buriahi, M. Chalermpon, Y. Rammah, Applied Physics A **126**, 1 (2020).
[15] G. Lakshminarayana, M. Dong, M. Al-Buriahi, A. Kumar, D.-E. Lee, J. Yoon et al., Applied Physics A **126**, 1 (2020).
[16] M. Kamislioglu, E. A. Guclu, H. Tekin, Applied Physics A **126**, 1 (2020).
[17] F. El-Agawany, K. Mahmoud, E. Kavaz, R. El-Mallawany, Y. Rammah, Applied Physics A **126**, 1 (2020).
[18] I. Boukhris, M. Al-Buriahi, H. Akyildirim, A. Alalawi, I. Kebaili, M. Sayyed, Ceramics International, 2020.
[19] I. Kebaili, I. Boukhris, M. Al-Buriahi, A. Alalawi, M. Sayyed, Ceramics International **47**, 1303 (2020).
[20] A. Srivastava, S. Sharma, N. Mehta, Journal of Environmental Chemical Engineering **7**, 103032 (2019).
[21] M. Emam-Ismail, E. R. Shaaban, M. El-Hagary, I. Shaltout, Philosophical Magazine 90 (25), 3499 (2010)
[22] Y. Rammah, A. Askin, A. Abouhaswa, F. El-Agawany, M. Sayyed, Applied Physics A **125**, 523 (2019).
[23] Y. Rammah, F. El-Agawany, I. El-Mesady, Applied Physics A **125**, 727 (2019).
[24] Y. Rammah, M. Sayyed, A. Ali, H. Tekin, R. El-Mallawany, Applied Physics A **124**, 832 (2018).
[25] F. El-Agawany, E. Kavaz, U. Perişanoğlu, M. Al-Buriahi, Y. Rammah, Applied Physics A **125**, 838 (2019).
[26] Y. Al-Hadeethi, M. Sayyed, Y. Rammah, Ceramics International **45**, 20724 (2019).
[27] A. Kumar, D. Gaikwad, S. S. Obaid, H. Tekin, O. Agar, M. Sayyed, Progress in Nuclear Energy **119**, 103047 (2020).
[28] E. Şakar, Ö. F. Özpolat, B. Alım, M. Sayyed, M. Kurudirek, Radiation Physics and Chemistry **166**, 108496 (2020).
[29] Y. Al-Hadeethi, M. Sayyed, Ceramics International **46**, 4795 (2020).
[30] A. Goel, E. R. Shaaban, M. J. Ribeiro, F. C. L. Melo, J. M. F. Ferreira Journal of Physics: Condensed Matter 19 (38), 386231 (2007).

[31] Z. A. Alrowaili, M. M. Soraya, T. A. Alsultani, Ammar Qasem, E. R. Shaaban, Mohammed Ezzeldien, Journal: Applied Physics A, DOI: 10.1007/s00339-020-04175-0
[32] E. R. Shaaban, M. Y. Hassaan, A. G. Mostafa, A. M. Abdel-Ghany, Journal of alloys and compounds 482 (1-2), 440 (2009).
[33] E. R. Shaaban, I. B.I Tomsah, Journal of thermal analysis and calorimetry 105 (1), 191 (2011).
[34] I. Han, L. Demir, Nuclear Instruments and Methods in Physics Research Section B: Beam Interactions with Materials and Atoms **267**, 3505 (2009).
[35] H. Manjunatha, Radiation Physics and Chemistry **137**, 254 (2017).
[36] Y. Harima, Nuclear Science and Engineering **83**, 299 (1983).
[37] ANSI/ANS-6.4.3. Gamma Ray Attenuation Coefficient and Buildup Factors for Engineering Materials. American Nuclear Society La Grange Park, IL, 1991
[38] J. I. Wood, Computational Methods in Reactor Shielding. Pergamon Press, 1982.
[39] A. B. Chilton, R. E. Faw, J. K. Shultis, Principles of Radiation Shielding Prentice-Hall, Englewood Cliffs, 1984
[40] M. F. Kaplan, Concrete Radiation Shielding: Nuclear Physics, Concrete Properties, Design and Construction. Longman Scientific & Technical, 1989.
[41] J. H. Hubbell, S. M. Seltzer, Tables Of X-Ray Mass Attenuation Coefficients And Mass Energy Absorption Coefficient 1 keV TO 20 MeV For Elements Z = 1 To 92 And 48 Additional Substance of Dosimetric Interest, Nist Research Information Center, 1995.
[42] SCHOTT. http://www.schott.com/advanced_optics/english/products/opticalmaterials/ special-materials/radiation-shielding-glasses/index.html. (Accessed at 1/12/2021).
[43] I. I. Bashter, Annals of Nuclear Energy **24**, 1389 (1997).